

Analyst

Accepted Manuscript



This is an *Accepted Manuscript*, which has been through the Royal Society of Chemistry peer review process and has been accepted for publication.

Accepted Manuscripts are published online shortly after acceptance, before technical editing, formatting and proof reading. Using this free service, authors can make their results available to the community, in citable form, before we publish the edited article. We will replace this *Accepted Manuscript* with the edited and formatted *Advance Article* as soon as it is available.

You can find more information about *Accepted Manuscripts* in the [Information for Authors](#).

Please note that technical editing may introduce minor changes to the text and/or graphics, which may alter content. The journal's standard [Terms & Conditions](#) and the [Ethical guidelines](#) still apply. In no event shall the Royal Society of Chemistry be held responsible for any errors or omissions in this *Accepted Manuscript* or any consequences arising from the use of any information it contains.

Cite this: DOI: 10.1039/c0xx00000x

www.rsc.org/xxxxxx

An Electrochemical and Computational Study for Discrimination of *D*- and *L*-Cystine by Reduced Graphene Oxide/ β -Cyclodextrin

Erhan Zor^{a,b,c,*}, Haluk Bingol^d, Almira Ramanaviciene^b, Arunas Ramanavicius^b, Mustafa Ersoz^e

Received (in XXX, XXX) Xth XXXXXXXXXX 20XX, Accepted Xth XXXXXXXXXX 20XX

DOI: 10.1039/b000000x

Here we report a novel enantioselective electrochemical biosensor for the discrimination of cystine enantiomers (*D*- and *L*-Cystine) using a chiral interface for specific recognition of *D*- and *L*-Cystine. The biosensor is based on reduced graphene oxide modified by β -cyclodextrin (*rGO*/ β -*CD*) at GCE surface. During the preparation of *rGO*/ β -*CD*/GCE, the modified electrode surfaces were characterized by cyclic voltammetry (CV), electrochemical impedance spectroscopy (EIS) and scanning electron microscopy (SEM). The electrochemical behaviours of the *D*- and *L*-Cystine were investigated using the *rGO*/ β -*CD*/GCE by CV and compared to bare GCE. A clear separation between the oxidation peak potentials of *D*- and *L*-Cystine was observed at 1.32 and 1.42 V, respectively. The electrochemical discrimination performance of the fabricated chiral sensor was also examined by differential pulse voltammetry (DPV) in mixed solution of *D*- and *L*-Cystine. In addition, DPV technique was used for the determination of *D*- and *L*-Cystine at the low concentration values in the range of 1.0-10.0 μ M. In order to investigate the amperometric response of *rGO*/ β -*CD*/GCE towards *D*- and *L*-Cystine, chronoamperometry technique was used in the concentration range of 10.0-100.0 μ M. The interactions of the enantiomers with *rGO*/ β -*CD* were modelled by molecular docking using AutoDock Vina and the interaction energies were predicted to be -4.8 and -5.3 kcal mol⁻¹ for *D*- and *L*-Cystine, respectively. The corresponding values of binding constants were calculated as 3.32×10^3 and 7.71×10^3 M⁻¹, respectively. The experimental and molecular docking results indicate that the *rGO*/ β -*CD*/GCE has different affinity for each enantiomer.

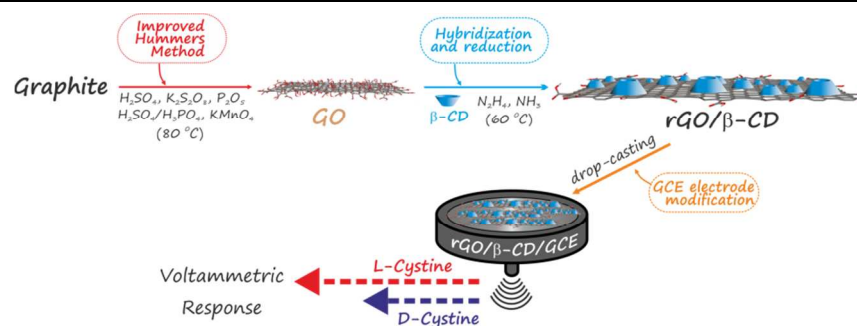
1. Introduction

Investigation of chiral compounds has a fundamental significance for understanding intrinsic properties of the biomolecular building blocks of life and broad classes of chemical processes occurring in living organisms.¹⁻³ Owing to this, distinction of chiral interactions is crucial in drug discovery, pharmaceutical and biochemical processes.⁴⁻⁶ Numerous compounds used in such areas are known to exist as mixture of enantiomers. One enantiomer may be ineffective or frequently possesses a different physiological role and may cause serious side-effects while the other may exhibit some desirable properties.⁷ Meanwhile, the development of simple, rapid, sensitive, highly selective, and not time-consuming methods for detection and quantification one individual enantiomer in very complex samples containing mixture of enantiomers still remains a challenge.^{8,9} While various techniques such as UV-vis spectroscopy,¹⁰ fluorescence spectroscopy,¹¹ high-performance liquid chromatography,¹² capillary electrophoresis¹³ and electrochemical^{14,15} have been performed for the detection of enantiomers of different compounds, a few studies have been successfully carried out by

electrochemical discrimination of enantiomers. For instance, Katakay and Lopes have achieved discrimination of facilitated chiral transfer of the ephedrinium ion at liquid-liquid interface,⁴ Nie et al. has prepared cysteine acid modified glassy carbon electrode to discriminate tyrosine enantiomers,¹⁶ and Zor et al. has developed an electrochemical biosensor based on the human serum albumin/graphene oxide/3-aminopropyltriethoxysilane modified indium tin oxide electrode for the discrimination of tryptophan enantiomers.⁷

In recent years, experimental studies combined with theoretical calculations have received increasing attention,¹⁷ because theoretical approaches can provide explanation of experimental observation.^{18,19} In this respect, molecular docking is one of the widely used molecular modeling methods in order to explain molecular recognition of the chiral molecules¹⁷ and it can provide an insight into the preferred binding location.²⁰

The key step for producing a chiral biosensor is to build a chiral surface having recognition sites with different affinity towards enantiomers.^{5,7} Such surface serves as a host for biologically active target compounds.²¹ Cyclodextrins (CDs) are a class of cyclic oligosaccharides, which are toroidal in shape with a hydrophobic inner cavity and a hydrophilic exterior.²²⁻²⁴



Scheme 1. Schematic diagram of producing electrochemical biosensor for the discrimination of Cystine enantiomers (*D*- and *L*-Cystine).

These interesting characteristics can provide them to bind selectively target molecules into their cavities through various kinds of intermolecular interactions such as hydrophobic interaction, Van der Waals force, electrostatic affinity, and hydrogen bond.²⁵ CDs can be attached on the surface of reduced graphene oxide (rGO) sheets not only to make graphene more hydrophilic but also to enable high surface area, and conductivity. Therefore, the integration of rGO and CD is expected to expand potential applications in various fields such as sensors, electrocatalysis and biological probe.²⁶ Recently, *rGO-CDs* modified electrodes have recently attracted great interest due to their potential application as selective and sensitive electrochemical biosensors.^{22,23,25,27,28}

Here we present the discrimination of two enantiomeric forms of cystine (*D*- and *L*-Cystine), which is a dimeric amino acid derivative and is a constituent of hair and nail keratin.²⁹ Chemical oxidation of disulfides such as cystine by bromine and other oxidizing agents is a well known commercial process.³⁰ However, to the best of our knowledge there is no prior report on the electrochemical enantiomeric discrimination of *D*- and *L*-Cystine by CV and DPV techniques. In order to achieve this, we prepared and characterized glassy carbon electrode surface modified with *rGO/β-CD* composite, and investigated the electrode performance electrochemically in detail. The interactions between Cystine enantiomers and *rGO/β-CD* were investigated by molecular docking studies due to the fact that it is a useful tool to confirm the binding mode, and the interaction energies were evaluated. The results show that the *rGO/β-CD/GCE* can be used as an effective electrochemical biosensor in order to discriminate *D*- and *L*-Cystine.

2. Experimental

2.1. Chemical and apparatus

All chemicals were of analytical grade and were used without further purification. Concentrated H_3PO_4 and H_2SO_4 , H_2O_2 (30%), hydrazine hydrate solution (50 wt %), ammonia solution (28 wt %), graphite powder (99.99 %), $\text{K}_2\text{S}_2\text{O}_8$, KMnO_4 (99%), P_2O_5 , *D*- and *L*-Cystine (cystine) and β -cyclodextrin were purchased from Sigma-Aldrich. All aqueous solutions were freshly prepared using ultra-pure water with a resistivity of 18.2 $\text{M}\Omega\text{cm}$.

Electrode morphologies were investigated by a scanning electron microscopy (SEM), performed on a ZEISS EVO LS 10 SEM at accelerating voltage of 20 kV and 5.00kX magnification. UV-vis absorption spectra were obtained on Shimadzu UV-1800

double beam spectrophotometer. Fourier transformed infrared (FT-IR) spectra of the samples were recorded between 550 and 4000 cm^{-1} using ATR FT-IR spectrometer (Perkin Elmer 100 FT-IR). Electrochemical impedance spectroscopy (EIS) measurements were conducted in A-PBS solution pH 7.01 containing 1.0 mM $[\text{Fe}(\text{CN})_6]^{3-/4-}$ redox couples. The impedance measurements were performed in the frequency range from 10 Hz to 100 kHz with 5 mV signal amplitude. Electrochemical measurements were performed in an electrochemical cell combined with a three-electrode configuration system using an Autolab PGSTAT 30 Potentiostat/Galvanostat operated by the GPES software Eco Chemie (Utrecht, Netherlands). Glassy carbon electrode (GCE), Ag/AgCl in saturated KCl ($\text{Ag}/\text{AgCl}/\text{KCl}_{\text{sat}}$) and platinum wire were used as working electrode, reference electrode and counter electrode, respectively. All measurements were carried out in a mixed solution of 50 mM sodium acetate and 50 mM phosphate buffer (A-PBS), pH 7.4, with 100 mM KCl at ambient temperature.

2.2. Preparation of β -Cyclodextrin Functionalized Graphene

Graphene oxide (GO) was synthesized from graphite powder by the improved method,³¹ which has significant advantages over Hummers' method,³² with an additional pre-oxidation process. Firstly, 3.0 g graphite was pre-oxidized in a mixture containing 15 mL concentrated H_2SO_4 , 1.5 g $\text{K}_2\text{S}_2\text{O}_8$ and 1.5 g P_2O_5 . The mixture was then diluted with ultra-pure water, filtered and dried in vacuum oven at 50 °C. Secondly, the pre-oxidized graphite was re-oxidized by improved method containing KMnO_4 (18.0 g) in a 9:1 mixture of concentrated $\text{H}_2\text{SO}_4/\text{H}_3\text{PO}_4$ (360:40 mL) for production of GO. β -cyclodextrin functionalized graphene was synthesized as indicated in literature as follows²²: Briefly, a 10.0 mL graphene oxide solution (0.5 mg/mL) was sonicated 1 h to obtain a homogeneous dispersion. Then, it was mixed with 10.0 mL of 40 mg/mL β -cyclodextrin aqueous solution and 150.0 μL of ammonia solution, followed by the addition of 10 μL of hydrazine solution. After shaken a few minutes, the solution was immersed in a water bath (60 °C) for 3.5 h to obtain a stable black dispersion. The dispersion was filtered to obtain reduced graphene oxide/ β -cyclodextrin nanocomposite (*rGO/β-CD*) which can be redispersed readily in water by ultrasonication.

2.3. Preparation of modified electrodes

Prior to modification, GCE surfaces were pre-cleaned with acetone, ethanol and ultra-pure water, respectively. Then, GCE surfaces were polished with 1.0, 0.3 and 0.05 μm alumina slurry (PACE Technologies, USA) on a felt pad, and washed with a

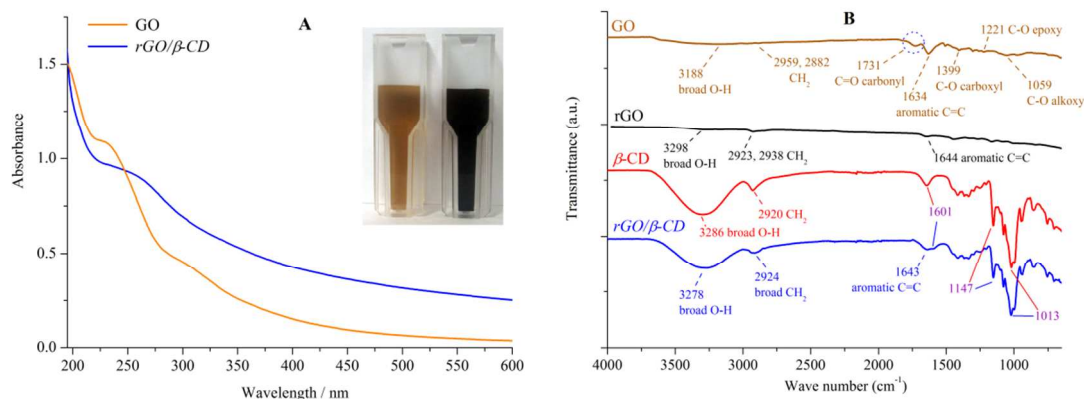


Fig. 1. UV-vis absorption spectra of GO and rGO. The inset shows photographs of GO (pale-brown) and rGO/ β -CD (black) (A). FT-IR spectra of GO, rGO, β -CD and rGO/ β -CD (B).

copious amount of ultra-pure water. The GCE was then immersed in water and methanol for 15 minutes, respectively, in an ultrasonic bath (Sonorex Super RK 106, Germany) in order to remove residual alumina particles by sonication. The electrode was dried at room temperature before the modification step. After drying, the rGO/ β -CD/GCE was prepared by casting 5.0 μ L of rGO/ β -CD suspension (0.2 mg/mL). Finally, the obtained electrode was dried at room temperature overnight. The rGO/ β -CD/GCE was then washed with ultra-pure water and dried before the use. A brief schematic diagram of producing electrochemical biosensor for discrimination of *D*- and *L*-Cystine was presented in Scheme 1.

2.4. Procedure for molecular docking study

The molecular docking studies were performed by ADVina considering the algorithm which maintains a rigid macromolecule while allowing ligand flexibility.³³ The crystal structure of β -CD was taken from the protein data bank. All hydrogen bonds for each rim of β -CD were oriented in the same direction.³⁴ The two-dimensional (2D) structures of GO, rGO, *D*- and *L*-Cys were drawn using ChemBioDraw v13.0. The starting geometries of GO and rGO were constructed considering the previous related literature.^{35–37} After the 2D sketches were converted to three dimensional (3D) images and the structures were energetically minimized, new coordinates were updated and recorded in PDB format with the help of Discovery Studio v3.5. The constructed graphene derivatives were assumed to be pristine and defect-, lesion-, and grain boundary-free.¹⁷ Before applying the molecular docking, the AutoDockTools version 1.5.6 (ADT) was used for optimization of the guest compounds from the PDB files by adding Gasteiger charges, assigning polar hydrogen atoms and setting up rotatable bonds. The pdbqt format files (required as input ADVina) were generated using ADT. The docking procedure was performed in two parts: Part 1; β -CD was docked to rGO using the following cartesian coordinates: $x=0$ Å, $y=0$ Å, $z=0$ Å. The molecular docking was carried out with a grid box size of 60 Å \times 70 Å \times 40 Å along the x , y , z axes with a grid spacing of 1.000 Å. Finally the lowest energy conformation was used for the docking analysis. Part 2; taking into account the docking conformation results of part 1, *D*- and *L*-Cystine were docked to rGO/ β -CD structure using the following cartesian coordinates:

$x=-2.560$ Å, $y=-3.560$ Å, $z=-14.500$ Å. A docking grid with a dimension of 14 Å \times 14 Å \times 20 Å and a grid spacing of 1.000 Å was applied for the second part of the molecular docking. All the other parameters were used as defined by ADVina for each docking steps. The resulting 9 binding models were further analyzed to find the most suitable binding model in each case. The preferred binding model having the minimum energy with the maximum number of poses clustered in that site was selected.³⁷ The ADVina output results were used for calculation of binding free energy change (ΔG_{bind}) and free energy change was further converted to the binding constants (K_{bind}) using $K_{bind}=\exp(\Delta G_{bind}/RT)$ at 25°C .

3. Results and discussion

3.1. Characterization of the rGO/ α -CD hybrid material

The obtained composite (rGO/ β -CD) was confirmed by the UV-vis and FT-IR spectral analysis. As shown in Fig. 1A, the GO dispersion displays a maximum absorption at 231 nm, which is due to the π - π^* transition of aromatic C=C bonds and a shoulder at 300 nm, which corresponds to the n - π^* transition of the C=O bond.³⁸ The color of the dispersion changed from pale-brown to black (Fig. 1A inset) and the absorption peak of the GO dispersion at 231 nm shifted to 264 nm suggesting that the conjugation within the rGO is formed due to the reduction by hydrazine.^{22,23,25}

The comparable FT-IR spectral features of GO, β -CD, rGO and rGO/ β -CD were presented in Fig. 1B. All spectra of the graphene derivatives have characteristic broad bands in the range of 3188 – 3278 cm^{-1} for O–H stretching vibration and the characteristic stretching vibrational modes around 1595 – 1644 cm^{-1} for C=C (aromatic) situated on the graphene sheet.^{22,39,40} After the reduction of GO to rGO sheet for rGO and rGO/ β -CD, whereas the peak intensity at 1731 cm^{-1} of C=O (carbonyl) was disappeared, the peaks at 1399 , 1221 and 1059 cm^{-1} for GO correspond to the C–O (carboxyl), C–O (epoxy) and C–O (alkoxy) functional groups greatly decreased.⁴⁰ These changes show that GO have been successfully reduced to rGO (or rGO/ β -CD).⁴¹ Also, the spectrum of rGO/ β -CD exhibits the characteristic β -CD absorption bands around 1601 , 1147 and 1013 cm^{-1} indicating the ring vibrations, which is clearly confirms that β -CD molecules are settled on rGO sheet.²²

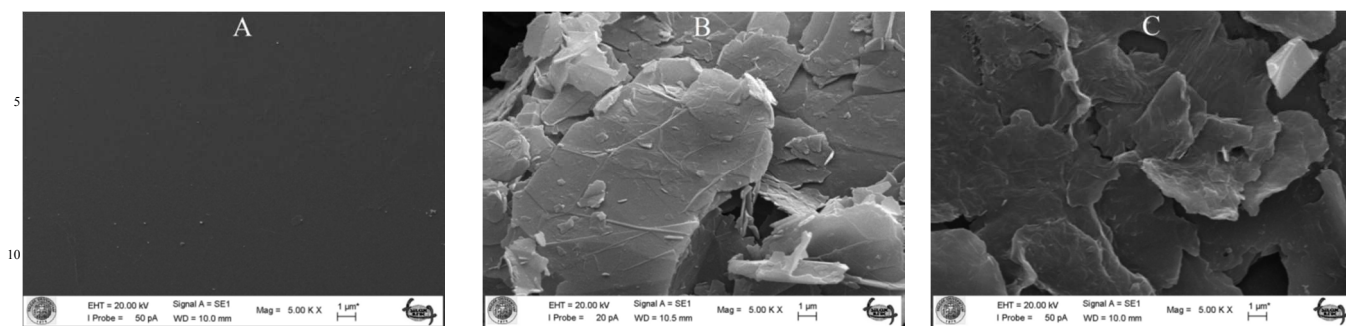


Fig. 2. SEM micrographs of GCE (A), *rGO*/GCE (B), and *rGO*/β-CD/GCE (C).

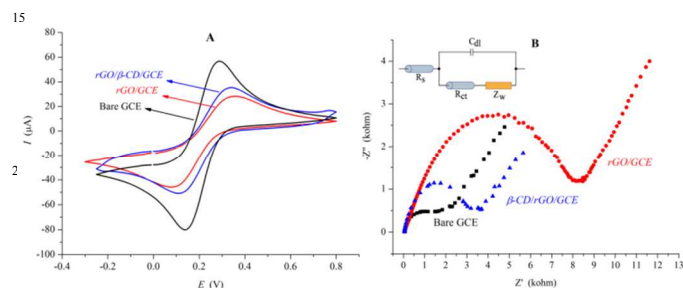


Fig. 3. Cyclic voltammograms (A) and Nyquist diagrams obtained at bare GCE, *rGO*/GCE and *rGO*/β-CD/GCE electrode in the presence of 1 mM $[\text{Fe}(\text{CN})_6]^{3-/4-}$ in A-PBS solution (pH 7.01) (B). The inset is Randle's equivalent circuit used to model impedance data in the presence of the redox couples.

3.2. Surface and electrochemical characterization of the modified electrodes

Scanning electron microscopy (SEM) was used to characterize the surface morphologies of bare GCE, *rGO* and *rGO*/β-CD modified GCE. The *rGO*/GCE surface exhibits that *rGO* sheets surround on the smooth surface of bare GCE electrode (Fig.2A) as can be seen in Fig.2B. Similar to *rGO* sheets, *rGO*/β-CD modified GCE surface displays a well coverage of the hybrid material as shown in Fig.2C.

CV and EIS were performed to investigate the electrochemical responses of the modified electrodes in A-PBS solution (pH 7.01) containing 1.0 mM $[\text{Fe}(\text{CN})_6]^{3-/4-}$. Fig.3A and 3B show the results of CV and EIS of the $[\text{Fe}(\text{CN})_6]^{3-/4-}$ redox couple for bare GCE, *rGO*/GCE and *rGO*/β-CD/GCE modified surfaces, respectively. While the bare GCE exhibits a well-defined redox peaks for the $[\text{Fe}(\text{CN})_6]^{3-/4-}$ in accordance with the literature,⁴² the modifications of the GCE surface with *rGO* and *rGO*/β-CD result in significant change on the electrochemical behaviors with decreases in the values of peak currents ratio ($I_{p,a}/I_{p,c}$) and increases in the values of the separation of peak potentials (ΔE_p).

According to related studies, these changes can be attributed to the presence of the film of graphene derivatives on electrode surface acts as an insulating layer, resulting in difficult interfacial electron transfer due to their disrupted sp^2 bonding networks.^{43,45} After the modifications of the GCE surface, the semicircle parts on the impedance spectrums increased as can be seen Fig. 3B. The obvious changes in the diameter in each modifications indicate that *rGO* decelerates the electron transfer of $[\text{Fe}(\text{CN})_6]^{3-/4-}$

because graphene derivatives act as a hindering layer for electron transfer as described above. The impedance values in the results of EIS were also fitted to standard Randle's equivalent circuit (the inset of Fig.3B) comprising of the charge transfer resistance (R_{ct}) on the electrode surfaces. The analyzed results also are tabulated in Table 1.

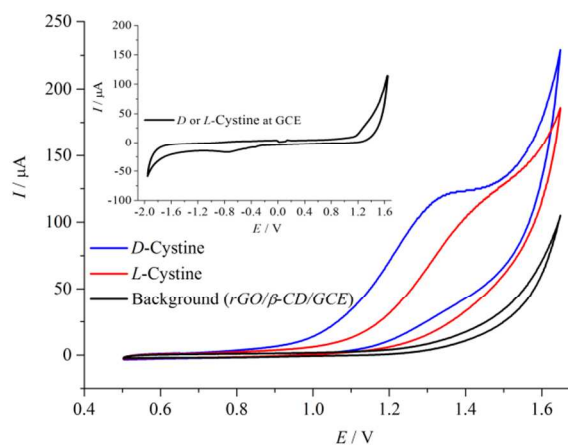
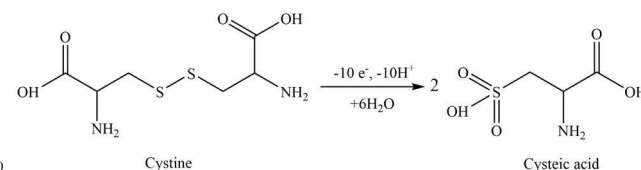


Fig. 4. Cyclic voltammograms in the absence and presence of D- and L-Cystine (50 μM) in A-PBS solution at *rGO*/β-CD/GCE. Potential sweep rate was 0.1 V s⁻¹.

Table 1 The results obtained from CV and EIS measurements for the electrodes

Electrode	$E_{1/2}$ (mV)	ΔE_p (mV)	$I_{p,a}/I_{p,c}$	R_{ct} (kohm)
Bare GCE	214	134	1.03	1.558
<i>rGO</i> /GCE	218	282	0.87	6.911
<i>rGO</i> /β-CD/GCE	223	232	0.93	2.114



Scheme 2. Possible oxidation mechanism of cystine to cysteic acid at *rGO*/β-CD/GCE.

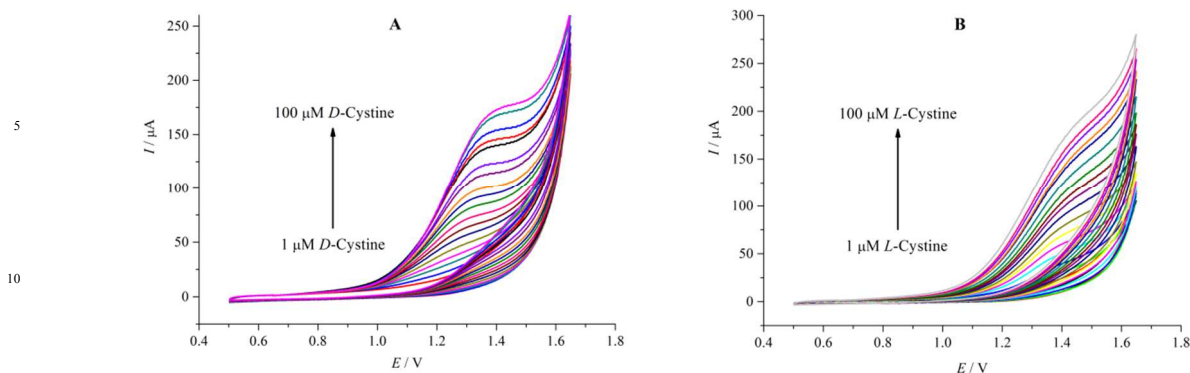


Fig. 5. Cyclic voltammograms at increasing concentration of D-Cystine (A) and L-Cystine (B) (1-100 μM) in A-PBS solution at rGO/β-CD/GCE. Potential sweep rate was 0.1V s⁻¹.

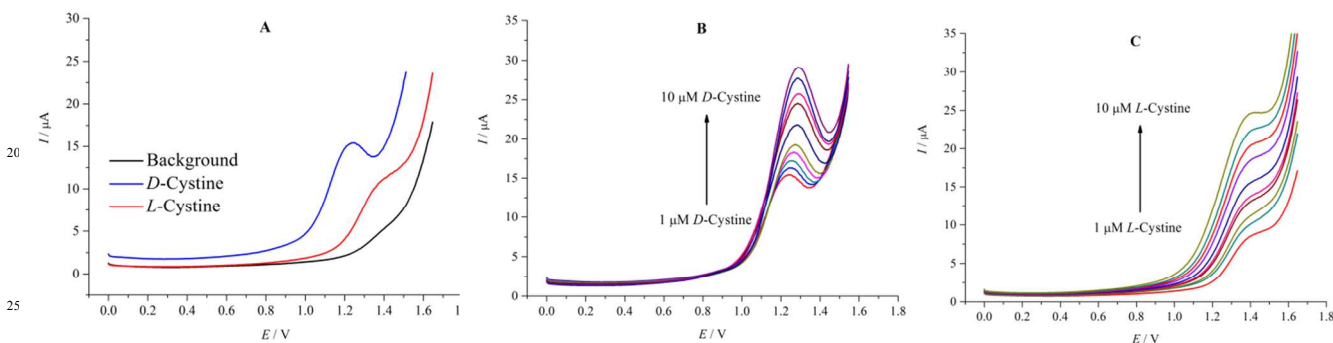


Fig. 6. Differential pulse voltammograms in the absence and presence of D- and L-Cystine in A-PBS solution (A). Differential pulse voltammograms at increasing concentration of D-Cystine (B) and L-Cystine (C) in low concentration range (1-10 μM) at rGO/β-CD/GCE. Potential sweep rate was 0.05 V s⁻¹.

3.3. Enantioselective discrimination of D- and L-Cystine at rGO/β-CD/GCE by voltammetry

Figure 4 shows the CV measurements performed with rGO/β-CD/GCE. No well-defined electrochemical response for the D- and L-Cystine was obtained at bare GCE (the inset), which is in accordance with the previous report¹⁶. After the modification of surface with rGO/β-CD, strong irreversible oxidation peaks of D- and L-Cystine were observed at different potential values of 1.32 and 1.42 V, respectively. The possible oxidation mechanism is provided in Scheme 2 as reported previously.³⁰

The voltammetric response of cystine oxidation to cysteic acid is changed according to enantiomeric structure. The high sensitivity and selective recognition capability of rGO/β-CD/GCE can be attributed to three factors: (i) the rGO/β-CD/GCE has larger surface area; (ii) the attached β-CD prevents the rGO to agglomerate; hence rGO/β-CD/GCE has more accessible active sites than bare GCE and respectively higher catalytic activity⁴⁶; (iii) these active sites of β-CD have different binding affinity towards target cystine enantiomers that might lead to the differences in the free Gibbs energy, this effect is observed as potential shift in electrochemical measurements¹⁶. The CV measurements present that by combining the unique electronic properties of rGO with the high selective β-CD compound, the rGO/β-CD nanocomposite shows significantly improved electrochemical sensing performance compared that to bare GCE.

Figures 5A and 5B show the additional CV measurements carried out in order to investigate the relationship between the peak current and the concentration in the range of 1-100 μM of

D- and L-Cystine. The oxidation current values increase with the increasing concentration of D- and L-Cystine. High oxidation potential values for corresponding concentrations were observed for L-Cystine. This can be attributed to that β-CD attached on rGO exhibits stronger interaction⁷ with L-Cystine than D-Cystine due to the more suitable match size, which has significant importance for enantioselective recognition.

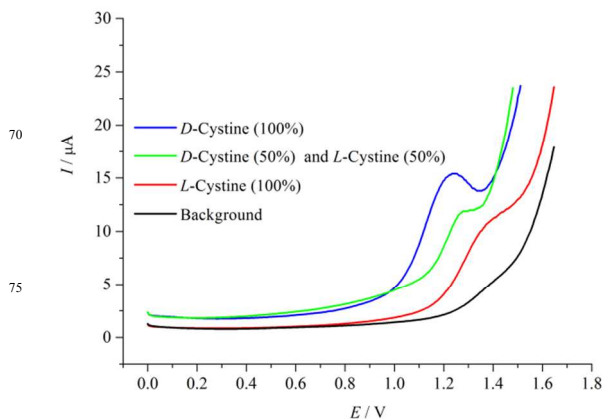


Fig. 7. Differential pulse voltammograms of enantiomeric mixtures of Cystine at different ratios of D- and L-Cystine (1:0, 1:1, and 0:1, c/c). Potential sweep rate was 0.05 V s⁻¹.

Figure 6A shows the DPV measurements for D- and L-Cystine at the rGO/β-CD/GCE. In accordance with CV measurements, well-defined peaks of D- and L-Cystine were observed at different potential values of 1.22 and 1.36 V, respectively. Figures 6B and 6C show the current change with the

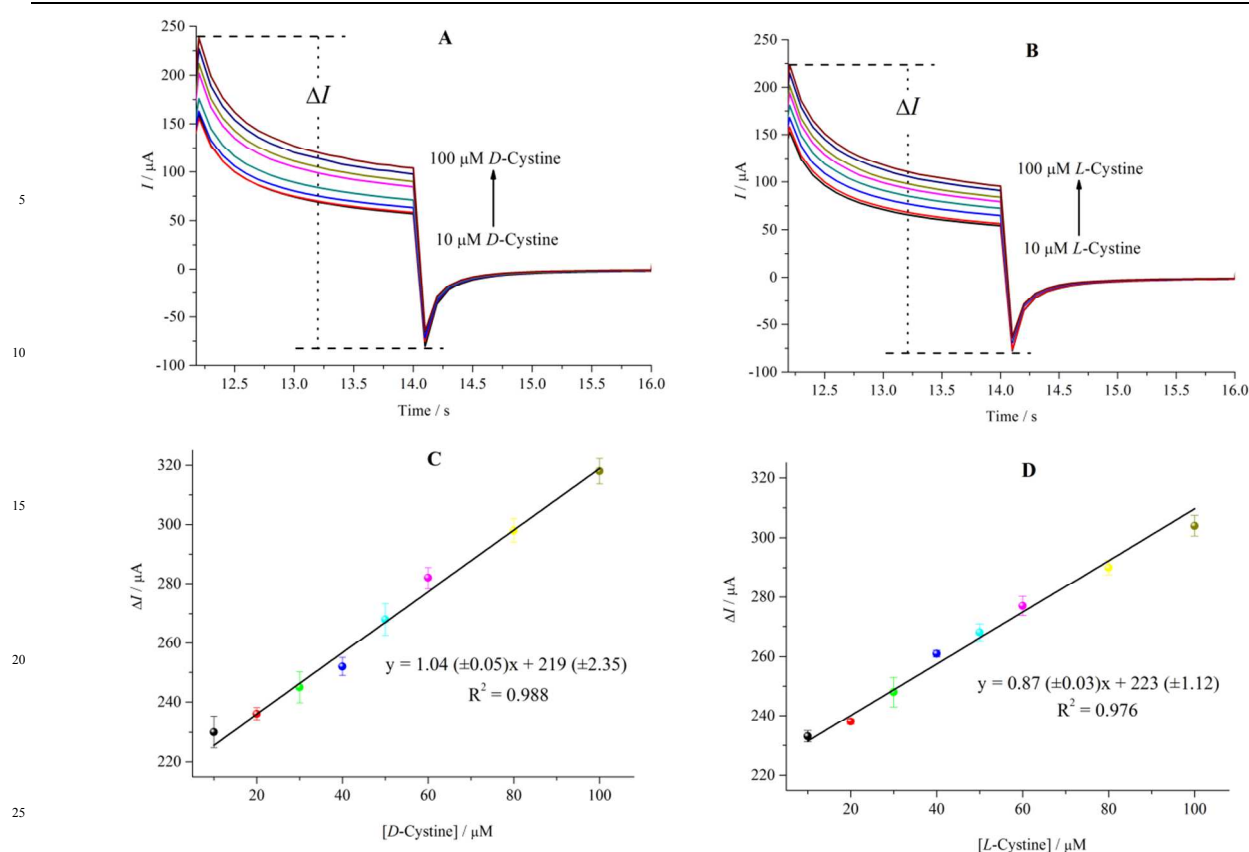


Fig. 8. Chronoamperograms at increasing concentration of *D*-Cystine (**A**) and *L*-Cystine (**B**) (10–100 μM) at *rGO*/ β -*CD*/*GCE*. The applied potentials are 0.00 and 1.32 V for *D*-Cystine, 0.00 and 1.42 V vs. Ag/AgCl (3 M KCl) for *L*-Cystine. **C** and **D** show the linear relationship between the enantiomer concentrations of Cystine and the oxidation peak currents.

increasing concentration of *D*- and *L*-Cystine, respectively. It can be also easily seen that the oxidation peak current of *D*- and *L*-Cystine also linearly increases with increasing concentration of *D*- and *L*-Cystine in the range of 1.0–10.0 μM .

Figure 7 shows differential pulse voltammograms for mixtures of *D*- and *L*-Cystine different ratios of (1:0, 1:1, and 0:1, c/c). As can be easily seen, the oxidation of 1:1 (c/c) enantiomeric mixture occurs at 1.27 V. This potential value is approximately mean of the oxidations of *D*- and *L*-Cystine enantiomers indicating clearly that there is a racemic mixture in the medium.

3.4. Amperometric responses of *rGO*/ β -*CD*/*GCE* for *D*- and *L*-Cystine

The amperometric responses of the *rGO*/ β -*CD*/*GCE* versus *D*- and *L*-Cystine concentration (10.0–100.0 μM) were investigated by chronoamperometry technique and results are shown in figure 8A and 8B. As it can be easily seen, *rGO*/ β -*CD*/*GCE* exhibited a good amperometric response to the increasing concentration of *D*- and *L*-Cystine with ΔI_{max} of 303.01 μA and 288.04 μA , respectively. In accordance with the CV and DPV measurements, amperometric results show that the oxidation peak current of *D*- and *L*-Cystine also linearly increases with increasing concentration of *D*- and *L*-Cystine in the range of 10.0–100.0 μM as presented in the in Figure 8C and 8D.

3.5. The stability, reproducibility and repeatability of the *rGO*/ β -*CD*/*GCE*

The reproducibility of the *rGO*/ β -*CD*/*GCE* was investigated by successive detection of 50.0 μM *D*- and *L*-Cystine with independently prepared three electrodes, and relative standard deviation (RSD) calculated as 2.45 % and 4.03%, respectively.

The repeatability of modified electrodes was evaluated by analysis of voltammetric responses three times by using the same electrode and relative standard deviations (RSD) were calculated as 3.28 % and 5.33 %, respectively.

The stability of the *rGO*/ β -*CD*/*GCE* was investigated by CV in a constant *D*- and *L*-Cystine concentration (50.0 μM) over a period of 2 weeks. It was observed that during first week the current responses almost remained stable and showed a decrease in current density about 12.13 % and 13.29 % of initial values at the end of 2 weeks. The decrease of current response may be attributed to the degradation of *rGO*/ β -*CD* sensing layer.

3.6. Molecular docking results

Besides the experimental studies of *D*- and *L*-Cystine with *rGO*/ β -*CD*, a molecular modeling simulation was also performed. Recently, there has been an increasing interest of molecular modeling studies on the recognition of a variety of molecules

with cyclodextrins for inclusion complexes and other aspects of supramolecular chemistry.¹⁹ In this respect, Zhang et al. depicted that the molecular modeling studies of host-guest interactions between CDs and enantiomers should provide better insights into these interactions and elucidate chiral recognition processes.¹⁹ Alvira has studied the separation of alanine enantiomers using β -CD by means of a molecular dynamics simulation and stated that β -CD is a good enantioselective chiral selector.⁴⁷ Herein, we aimed to study theoretically inclusion complex formation and to predict the preferentially recognition of *D*- and *L*-Cystine to *rGO*/ β -CD. The molecular docking studies were performed in two parts by employing ADV. In the first part of the docking process, β -CD was docked to GO as indicated in our previous paper for α -CD.¹⁷ Similar to α -CD, β -CD also preferentially settled on the basal plane of GO from the wide rim which has distinctly hydrophilic character^{17,18} (Fig. 9A). The overall binding energy of β -CD on GO for this docking process was calculated as $-9.5 \text{ kcal mol}^{-1}$. Fig. 9B shows the *rGO*/ β -CD structure after reduction of residual oxygen containing groups of GO by a reducing agent as indicated in experimental part.

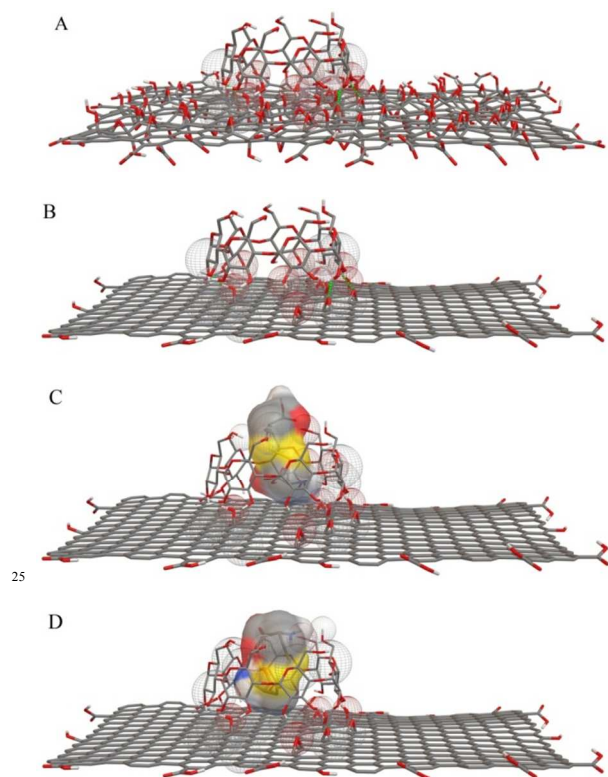


Fig. 9. Overall structures of β -CD in complexes with GO (A) and *rGO* (B) represented as stick models. Side view stick model of schematic drawing for the *rGO*/ β -CD complex with *D*-Cystine (C) and *L*-Cystine (D), respectively.

In the second part, the docking models were evaluated for the preferentially recognition of *D*- and *L*-Cystine to *rGO*/ β -CD. Figures 9C and 9D show the docked models in which *D*- and *L*-Cystine penetrate through the cavity of β -CD. The overall binding energies for the recognition of *D*- and *L*-Cystine to *rGO*/ β -CD

were predicted as -4.8 and $-5.3 \text{ kcal mol}^{-1}$, respectively. Considering the overall binding energies, the binding constants were calculated as 3.32×10^3 and $7.71 \times 10^3 \text{ M}^{-1}$, respectively, resulting in a high chiral discrimination with a ratio of $K_L/K_D = 2.32$. According to "three-point interaction" theory pointed out by Dalglish in 1952,⁴⁸ at least three configuration-dependent points are needed for the recognition between chiral selectors and enantiomeric analytes, and one of them must be an enantioselective interaction.⁴⁹ Herein, the different binding constants values can be attributed to the enantioselective binding affinity of β -CD. In other words, β -CD provides a chiral environment exhibiting various noncovalent interactions, such as van der Waals interactions, hydrophobic interactions and hydrogen bonding, which play a pivotal role for chiral discrimination. As a result of much more interactions are occurred for *L*-Cystine, *rGO*/ β -CD has the higher binding energy than *D*-Cystine. The higher binding energy and binding constant for occurring interaction between *L*-Cystine and *rGO*/ β -CD are consistent with the electrochemical results indicating the higher binding affinity of *rGO*/ β -CD for *L*-Cystine, and also provide a better insight into the interactions between cystine enantiomers and *rGO*/ β -CD on a molecular level.

Conclusions

In the present work, we report a simple and fast method for the discrimination of *D*- and *L*-Cystine by *rGO*/ β -CD/GCE electrode. In the experimental part of the study, CV, DPV and chronoamperometry techniques were employed to investigate the electrochemical response of the modified electrode for the discrimination of *D*- and *L*-Cystine. Enantioselective properties of β -CD provides opportunity for the discrimination of *D*- and *L*-Cystine. *rGO* layer provides a large surface area for the deposition of β -CD. The described method is very simple, cheap and not time consuming. To the best of our knowledge, it is the first report on electrochemical chiral sensor for the discrimination of *D*- and *L*-Cystine. In the second part of the study, molecular interactions were investigated by molecular docking in order to compare the experimental results with the computational results. The molecular docking results supported the electrochemical results indicating the different enantioselective affinity of *rGO*/ β -CD towards *D*- and *L*-Cystine. As a consequence, this study is expected to be a useful and promising platform in sensor area for electrochemical discrimination of some chiral analytes.

Acknowledgements

This work was supported by TÜBİTAK (113Z664) and was produced from a part of E. Zor's PhD Thesis. We also express our deep thanks to the Turkish Academy of Sciences (TUBA).

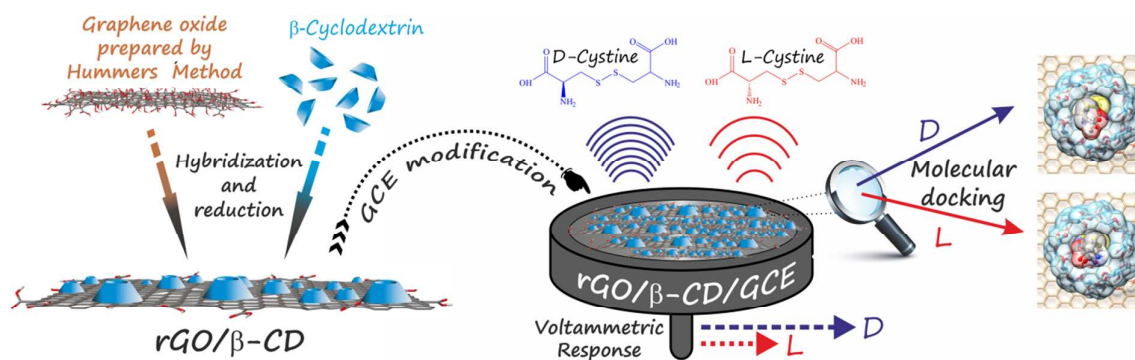
Notes and references

^a Selçuk University, Institute of Science, Department of Chemistry, Konya, Turkey. Tel.: +90 332 3238220 - 5566, Fax: +90 332 3238225. E-mail: zorerhan@gmail.com

^b Vilnius University, Faculty of Chemistry, Centre of Nanotechnology and Materials Science, Vilnius, Lithuania. E-mail: almyra@imi.lt, arunas.ramanavicius@chf.vu.lt

- ^c Necmettin Erbakan University, A.K. Education Faculty, Science and Technology Department, Konya, Turkey.
- ^d Necmettin Erbakan University, A.K. Education Faculty, Chemistry Department, Konya, Turkey. E-mail: halukbingol@gmail.com
- ^e Selcuk University, Advanced Technology Research and Application Center, Konya, Turkey, E-mail: ersozm@gmail.com
- 1 M. Trojanowicz and M. Kaniewska, *Electroanalysis*, 2009, **21**, 229–238.
- 2 L. Wu and F. G. Vogt, *J. Pharm. Biomed. Anal.*, 2012, **69**, 133–147.
- 3 L. Song, S. Wang, N. A. Kotov and Y. Xia, *Anal. Chem.*, 2012, **84**, 7330–7335.
- 4 R. Katakay and P. Lopes, *Chem. Commun.*, 2009, **12**, 1490–1492.
- 5 Q. Zhang, L. Guo, Y. Huang, Y. Wang, Q. Han and Y. Fu, *Anal. Methods*, 2013, **5**, 4397–4401.
- 6 Y. Tao, N. R. Quebbemann and R.R. Julian, *Anal. Chem.*, 2012, **84**, 6814–6820.
- 7 E. Zor, I. Hatay Patir, H. Bingol and M. Ersoz, *Biosens. Bioelectron.*, 2013, **42**, 321–325.
- 8 D. Patterson, M. Schnell and J.M. Doyle, *Nature*, 2013, **497**, 475–477.
- 9 L. Challier, F. Mavré, J. Moreau, C. Fave, B. Schollhorn, D. Marchal, E. Peyrin, V. Noel and B. Limoges, *Anal. Chem.*, 2012, **84**, 5415–5420.
- 10 J. Athilakshmi, M. Mohan and D. K. Chand, *Tetrahedron Lett.*, 2013, **54**, 427–430.
- 11 Z. Huang, S. Yu, K. Wen, X. Yu and Lin Pu, *Chem. Sci.*, 2014, **5**, 3457–3462.
- 12 L. Qin, X-W. Hea, W-Y. Li and Y-K. Zhang, *J. Chromatogr. A*, 2008, **1187**, 94–102.
- 13 L. Sánchez-Hernández, M. L. Marina and A. L. Crego, *J. Chromatogr. A*, 2011, **1218**, 4944–4951.
- 14 Y. Wang, L. Luo, Y. Ding, X. Zhang, Y. Xu and X. Liu, *J. Electroanal. Chem.*, 2012, **667**, 54–58.
- 15 E. Khaled, M. S. Kamel, H. N. A. Hassan and H. Y. Aboul-Enein, *J. Electroanal. Chem.*, 2011, **661**, 239–244.
- 16 R. Nie, X. Bo, H. Wang, L. Zeng and L. Guo, *Electrochem. Commun.*, 2013, **27**, 112–115.
- 17 E. Zor, M. E. Saglam, Sabri Alpaydin and Haluk Bingol, *Anal. Methods*, 2014, **6**, 6522–6530.
- 18 K. B. Lipkowitz, *Chem. Rev.*, 1998, **98**, 1829–1873.
- 19 X-H. Zhang, H-L. Wu, X-L. Yin, L-H. Li, J-Y. Wang, Y. Chen, C. Kang and Ru-Qin Yu, *Anal. Methods*, 2013, **5**, 710–717.
- 20 X. Li, G. Wang, D. Chen and Y. Lu, *RSC Adv.*, 2014, **4**, 7301–7312.
- 21 L. Szente and J. Szemán, *Anal. Chem.*, 2013, **85**, 8024–8030.
- 22 Y. Guo, S. Guo, J. Ren, Y. Zhai, S. Dong and E. Wang, *ACS Nano*, 2010, **4**, 4001–4010.
- 23 Y. Guo, S. Guo, J. Li, E. Wang and S. Dong, *Talanta*, 2011, **84**, 60–64.
- 24 Z. Wang, S. Xiao and Y. Chen, *J. Electroanal. Chem.*, 2006, **589**, 237–242.
- 25 D. Lu, S. Lin, L. Wang, X. Shi, C. Wang and Y. Zhang, *Electrochim. Acta*, 2012, **85**, 131–138.
- 26 M. Chen, Y. Meng, W. Zhang, J. Zhou, J. Xie and G. Diao, *Electrochim. Acta*, 2013, **108**, 1–9.
- 27 C. Xu, X. Wang, J. Wang, H. Hu and L. Wan, *Chem. Phys. Lett.*, 2010, **498**, 162–167.
- 28 Q. Han, Y. Wang, Y. Huang, L. Guo and Y. Fu, *Analyst*, 2013, **138**, 2051–2056.
- 29 A. Nosal-Wiercinska, *Electrochim. Acta*, 2013, **92**, 397–403.
- 30 K. Firoz Babu, R. Sivasubramanian, M. Noel and M. Anbu Kulandainathan, *Electrochim. Acta*, 2011, **56**, 9797–9801.
- 31 D. C. Marcano, D. V. Kosynkin, J. M. Berlin, A. Sinitiskii, Z. Sun, A. Slesarev, L. B. Alemany, W. Lu and J. M. Tour, *ACS Nano*, 2010, **4**, 4806–4814.
- 32 W. S. Hummers and R. E. Offeman, *J. Am. Chem. Soc.*, 1958, **80**, 1339–1339.
- 33 O. Trott and A. J. Olson, *J. Comput. Chem.*, 2010, **31**, 455–461.
- 34 J. Köhler and N. Grczelschak-Mick, *Beilstein J. Org. Chem.* 2013, **9**, 118–134.
- 35 S. Mao, H. Pu and J. Chen, *RSC Adv.*, 2012, **2**, 2643–2662.
- 36 Y. Zhang, C. Wu, S. Guo and J. Zhang, *Nanotechnol. Rev.*, 2013, **2**, 27–45.
- 37 G. P. Kotchey, B. L. Allen, H. Vedala, N. Yanamala, A. A. Kapralov, Y. Y. Tyurina, J. Klein-Seetharaman, V. E. Kagan and A. Star, *ACS Nano*, 2011, **5**, 2098–2108.
- 38 J-L. Chen, X-P. Yan, K. Meng, and S-F. Wang, *Anal. Chem.*, 2011, **83**, 8787–8793.
- 39 E. Zor, M. E. Saglam, I. Akin, A. O. Saf, H. Bingol and Mustafa Ersoz, *RSC Adv.*, 2014, **4**, 12457–12466.
- 40 V. Chandra and K. S. Kim, *Chem. Commun.*, 2011, **47**, 3942–3944.
- 41 X. Gao, J. Jang and S. Nagase, *J. Phys. Chem. C*, 2010, **114**, 832–842.
- 42 F. C. Moraesa, I. Cesarinoa, V. Cesarinoa, L. H. Mascarob and S. A. S. Machado, *Electrochim. Acta*, 2012, **85**, 560–565.
- 43 Y. Hu, K. Wang, Q. Zhang, F. Li, T. Wu and L. Niu, *Biomaterials*, 2012, **33**, 1097–1106.
- 44 Y. Hu, F. Li, X. Bai, D. Li, S. Hua, K. Wang and L. Niu, *Chem. Commun.*, 2011, **47**, 1743–1745.
- 45 E. Zor, A. O. Saf, H. Bingol and M. Ersoz, *Anal. Biochem.*, 2014, **449**, 83–89.
- 46 L. Tan, K-G. Zhou, Y-H. Zhang, H-X. Wang, X-D. Wang, Y-F. Guo and H-L. Zhang, *Electrochem. Commun.*, 2010, **12**, 557–560.
- 47 E. Alvira, *Tetrahedron: Asymmetr.* 2013, **24**, 1198–1206.
- 48 C. E. Dalglish, *J. Chem. Soc.*, 1952, 3940–3942.
- 49 C. Chang, X. Wang, Y. Bai and H. Liu, *Trend. Anal. Chem.*, 2012, **39**, 195–206.

Graphical and Textual Abstract



This study indicates applicability of two different techniques (electrochemical, and computational study) for discrimination of cystine enantiomers (*D*- and *L*-Cystine) by reduced graphene oxide/ β -cyclodextrin (*rGO*/ β -*CD*) hybrid material.

Keywords: Chiral sensor, Enantioselectivity, β -Cyclodextrin, Reduced-Graphene oxide, Cystine discrimination, molecular docking.